Available online at www.sciencedirect.com
SCIENCE DIRECT®
Chemical Physics 291 (2003) 61–72
Chemical Physics
www.elsevier.com/locate/chemphys

On the energy dependence of the Zeeman and hyperfine parameters in the $\tilde{A}^2\Sigma^+$ state of OH and OD

Ju Xin [a], Ionela Ionescu [b], David Kuffel [b], Scott A. Reid [b,*]

[a] Department of Physics and Engineering Technologies, Bloomsburg University, Bloomsburg, PA 17815, USA
[b] Department of Chemistry, Marquette University, P.O. Box 1881, Milwaukee, WI 53201-1881, USA

Received 13 March 2003

Abstract

We report quantum beat studies of the energy dependence of the Zeeman parameters in the $\tilde{A}^2\Sigma^+$ state of OH and OD, and the nuclear hyperfine parameters of OD($\tilde{A}^2\Sigma^+$). In contrast to previous work, we find that the sign and magnitude of the anisotropic g-factor g_l for $v' = 0$ is consistent with that expected from Curl's relationship. However, at higher energies g_l changes sign, a result we attribute to interaction with the repulsive $1^4\Pi$ state, which is known to lead to predissociation at higher energies. The magnetic and electric quadrupole hyperfine constants were determined for OD($\tilde{A}^2\Sigma^+, v' = 0$–3), and the constants for $v' = 2, 3$ are reported here for the first time. The derived values are consistent with previous experimental results and available ab initio calculations.

1. Introduction

The hydroxyl radical is an important species in atmospheric and combustion chemistry and astrophysics [1,2], and the subject of numerous experimental [3–56] and theoretical [57–74] investigations. Much of this work has focused on the ultraviolet $\tilde{A}^2\Sigma^+ \leftarrow \tilde{X}^2\Pi$ system, which was observed in flames and electric discharges more than 80 years ago [2]. The $\tilde{A}^2\Sigma^+$ state correlates with $O(^1D) + H(^2S)$ products, and is crossed by several repulsive states ($^2\Sigma^-$, $^4\Sigma^-$, $^4\Pi$) correlating with $O(^3P) + H(^2S)$, [41] providing a classic example of Case I predissociation [2]. Experimental studies [41,46,50,52,55] show that for low N the onset of predissociation occurs at $v' = 2$ for OH and $v' = 3$ for OD, and the trends in lifetime as a function of excited rotational and vibrational state are well reproduced by ab initio calculations [67,73,74]. At higher energies, theoretical studies [68–72] predict that interferences among direct and indirect pathways will lead to asymmetric (Fano) lineshapes and a pronounced wavelength dependence of the product yields, which has been observed experimentally in only a few cases [75–80]. Thus, experimental and theoretical interest in this molecule continues to this day.

Spectroscopic studies of the $\tilde{A}^2\Sigma^+ \leftarrow \tilde{X}^2\Pi$ system have examined the rotational and fine structure

* Corresponding author. Tel.: +414-288-7565; fax: +414-288-7066.
E-mail address: scott.reid@mu.edu (S.A. Reid).

0301-0104/03/$ - see front matter © 2003 Elsevier Science B.V. All rights reserved.
doi:10.1016/S0301-0104(03)00184-8

[9,27], hyperfine structure [25,26,33,39,40,42,44, 54], and Zeeman [22,25,26,33,38,40,42,53,54] and Stark [23,26] effects. Metcalf and co-workers [15,22] used the Hanle effect, level crossing spectroscopy, and optical double resonance to determine Landé g-factors for some rotational levels in $\tilde{A}^2\Sigma^+(v' = 0)$. Zare and co-workers [16,25,26] employed zero- and high-field level crossing and optical-radio frequency double resonance to determine the OD hyperfine constants, radiative lifetime and Landé g-factors in $\tilde{A}^2\Sigma^+(v' = 0)$, and conducted Stark measurements to determine the excited state dipole moment [26]. Subsequently, Metcalf and co-workers [38,40,42] applied the quantum beat technique to measure Landé g-factors for OH $\tilde{A}^2\Sigma^+(v' = 0)$, and the same method was used by Carter et al. [54] to probe the $\tilde{A}^2\Sigma^+(v' = 0)$ level of OD and the OD · Ar van der Waals complex. The ensuing years have witnessed increasingly precise measurements of the hyperfine parameters for the $v' = 0,1$ levels in the $\tilde{A}^2\Sigma^+$ state of OH and OD [39,44,54], which are in reasonable agreement with available ab initio predictions [59].

In light of these studies, it is surprising that fundamental questions remain regarding the Zeeman parameters of the $\tilde{A}^2\Sigma^+$ state. For example, Coxon conducted a two-state fit of the measured spectrum for the $\tilde{A}^2\Sigma^+ \leftarrow \tilde{X}^2\Pi$ system of OD [30], and found that the spin–rotation splittings in the $\tilde{A}^2\Sigma^+$ state of OD arose predominantly from a second order spin–orbit interaction with $\tilde{X}^2\Pi$ (a case of "pure precession"). Therefore, Curl's relationship [81] for the anisotropic correction to the electron spin g-factor, g_l, should approximately hold. However, a recent quantum beat study [54] of OD($\tilde{A}^2\Sigma^+$, $v' = 0$) determined a value of the correct sign but an order of magnitude larger than expected from Curl's relationship. In addition, the reported electron spin g-factor was significantly larger than the free electron value. These results were attributed to mixing with excited quartet states [54]. We find this surprising, in that the $\tilde{A}^2\Sigma^+(v' = 0)$ level of OD lies $\sim$4000 cm^{-1} below the opening of the lowest dissociation channel, and $\sim$24 000 cm^{-1} below the lowest lying quartet state ($^4\Sigma^-$) in the Franck–Condon region [67]. Moreover, such an effect should also be found for OH($\tilde{A}^2\Sigma^+, v' = 0$), which is not the case [42]. Thus, there is a need for further studies of the Zeeman effect in the $\tilde{A}^2\Sigma^+$ state and its energy dependence.

Our group has been interested for several years in the application of high-resolution quantum beat methods to free radicals [82–85]. The quantum beat method offers the advantages of other coherent time-domain spectroscopies [86], with an intrinsic resolution ($\sim$160 kHz for a radiative lifetime of 1 μs) capable of revealing molecular hyperfine structure and splittings induced by weak magnetic or electric fields. As a prelude to the application of quantum beat methods to polyatomic radicals, and in view of the unanswered questions regarding the Zeeman parameters in the $\tilde{A}^2\Sigma^+$ state, we undertook a detailed study of the energy dependence of the Zeeman parameters for both OH and OD, and also report the magnetic and electric quadrupole hyperfine constants for OD ($v' = 0$–3).

2. Experimental procedure

2.1. Experimental apparatus

The apparatus consisted of a cubic, black-anodized vacuum chamber evacuated by a 6 in. diffusion pump (Varian VHS-6) and equipped with a molecular beam source and fluorescence detection assembly. The chamber was surrounded by a triaxial Helmholtz coil system (Walker Scientific) used to null the earth field and generate fields for Zeeman experiments. Power to each coil came from independent power supplies (Kepco), and the field strength was calibrated using a Hall effect Gaussmeter. The field vector was oriented along the detection (space fixed X) axis, perpendicular both to the direction of laser propagation (along the space fixed Y axis) and to the polarization axis of the linearly polarized laser beam (oriented along the space fixed Z axis). In this configuration the selection rule for Zeeman quantum beats is: $\Delta M_F = \pm 2$.

The laser system consisted of a tunable, frequency doubled, etalon narrowed dye laser (Lambda-Physik Scanmate 2E) pumped by the second (532 nm) or third (355 nm) harmonic of a Nd:YAG laser (Continuum Powerlite 7010). The following dyes or dye combinations were used: R640/R610 (OH and OD, $v' = 0$), R6G (OH and

OD, $v' = 1$), C540 (OD, $v' = 2$), C307 (OD, $v' = 3$; OH, $v' = 2$). The laser output passed through a linear polarizer (CVI laser, 10^5:1 extinction) prior to entering the chamber. Typical pulse energies were 10–200 μJ, and the unfocused beam was of ~3 mm diameter. The pulse energy was increased with increasing v' to offset the decreasing Franck–Condon factor.

The OH (OD) radicals were generated by a pulsed electrical discharge through a mixture of H_2O (D_2O) in Argon, generated by passing Ar at a typical backing pressure of 20 psig through a bubbler containing H_2O (D_2O) at room temperature. The mixture was expanded into vacuum via a commercial pulsed valve (General Valve IOTA-1), modified by the addition of a ring electrode discharge assembly [87]. The discharge was initiated by a negative going 800 V pulse of ~20 μs duration, which passed through a 10 kΩ ballast resistor, and was set near the falling edge of the gas pulse to minimize the effects of the transient magnetic field generated by the (magnetically activated) valve. The timing of laser, nozzle, and discharge firing was controlled via a digital delay generator (Stanford Research Systems DG535), which generated the gate pulse for the high voltage pulser (Directed Energy GRX-1.5K-E). The laser beam crossed the molecular beam at a distance of ~15 mm (30 nozzle diameters) downstream. Fluorescence was collected at right angles to both the laser and molecular beam by a two lens $f/2.4$ condenser assembly, and passed through a UV polarizer (Meadowlark Optics) prior to striking a photomultiplier tube detector (Orion) held at typically −550 V. The PMT output was terminated into 50 Ω and digitized by an oscilloscope (HP 54521A) operated at a sampling rate of 1 GHz and record length of 4096 points.

Under typical experimental conditions, the OH (OD) radicals were produced almost exclusively in the $J = 3/2$ level of the $^2\Pi_{3/2}$ state, and we estimate a rotational temperature of ≈10 K from a comparison of intensity ratios for $R_{21}(2)/R_{21}(1)$ and $R_{11}(2)/R_{11}(1)$ pairs. Zeeman quantum beats were observed on the $S_{21}(1)$, $R_{21}(1)$, $R_{11}(1)$, and $Q_{11}(1)$ transitions, which provided access to excited state levels with $N = 1$–3 and $J = 3/2$–5/2. Transition frequencies were obtained from [9,27].

2.2. Data collection and analysis procedures

Pairs of waveforms were collected at a given magnetic field strength for parallel and perpendicular orientations of the detector polarization with respect to the polarization axis of the laser, achieved by rotating a linear ultraviolet (UV) polarizer (Meadowlark Optics) placed between the condenser lens system and PMT. The waveforms were typically averaged over 2500 laser shots. The time-dependent degree of polarization [$P(t)$] was calculated for each pair according to the equation:

$$P(t) = \frac{I_{\parallel}(t) - I_{\perp}(t)}{I_{\parallel}(t) + I_{\perp}(t)}. \quad (1)$$

Fig. 1 displays representative data for the $R_{21}(1)$ transition in the $v' = 1 \leftarrow v'' = 0$ band of OH at a field strength of 2.72 G. The upper panel displays the waveforms, and the lower panel the calculated degree of polarization. Consistent with the theory of anisotropic quantum beats, the modulations in

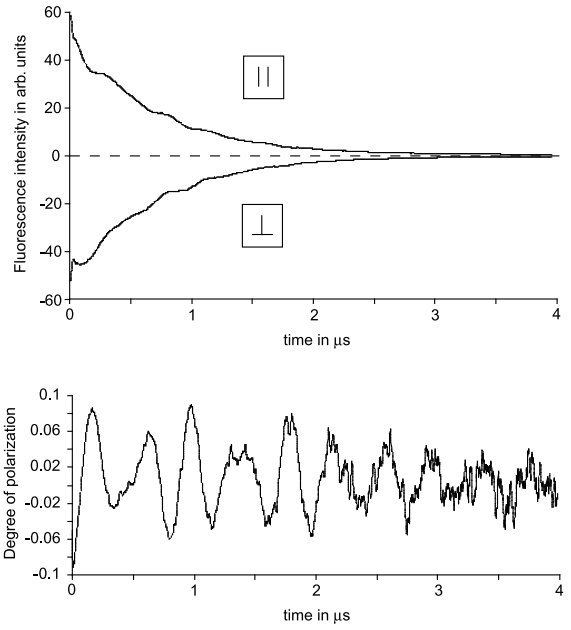

Fig. 1. Upper panel: Waveforms observed following excitation of the $R_{21}(1)$ transition in the $v' = 1 \leftarrow v'' = 0$ band of OH at a magnetic field strength of 2.72 G, obtained in parallel (top) and perpendicular (bottom) orientations of laser and detection polarizations. Lower panel: Degree of polarization calculated following Eq. (1) in the text.

the two waveforms exhibit a phase shift of 180°, and reduced amplitude for the perpendicular configuration.

The Fourier transform of $P(t)$ was obtained using PSIplot software. Fig. 2 displays the transform of the $P(t)$ shown in Fig. 3, which reveals two strong quantum beats. The center frequencies were obtained by fitting each peak to a Gaussian function using the Marquardt–Levenburg method. We tested both Gaussian and Lorentzian functions, and obtained similar goodness-of-fit statistics for isolated peaks. The fits to a Gaussian function typically gave correlation coefficients $\geqslant 0.999$, with a typical standard deviation of 30 kHz in the determined peak center frequency. This procedure was repeated for 8–10 different field strengths in the range over which linear tuning was observed. For OH, this range extended to the highest fields used (~10 G), while for OD to fields below ~5 G, consistent with the observations of Zare and co-workers [16,25,26]. Beats arising from different hyperfine components (inter-manifold beats) were not observed for OH, as the hyperfine splittings are much larger than the coherence width of our laser [44]. Thus, the Landé factor for a given F component was determined by a linear fit of the magnetic field dependence of the intra-manifold beat frequency using the formula:

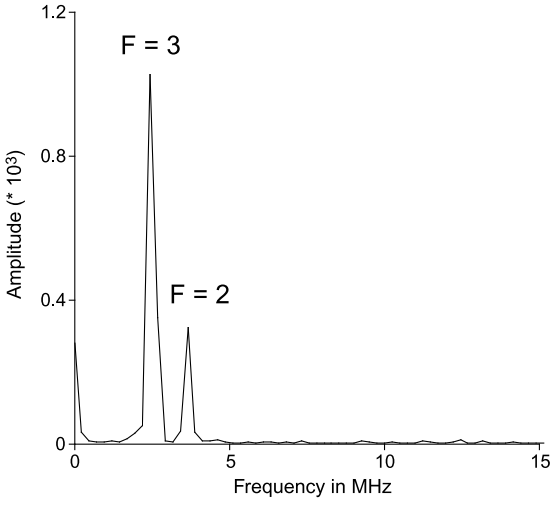

Fig. 2. Fourier transform of the degree of polarization data shown in bottom panel of Fig. 1. The beats are labeled in terms of the excited state hyperfine quantum number.

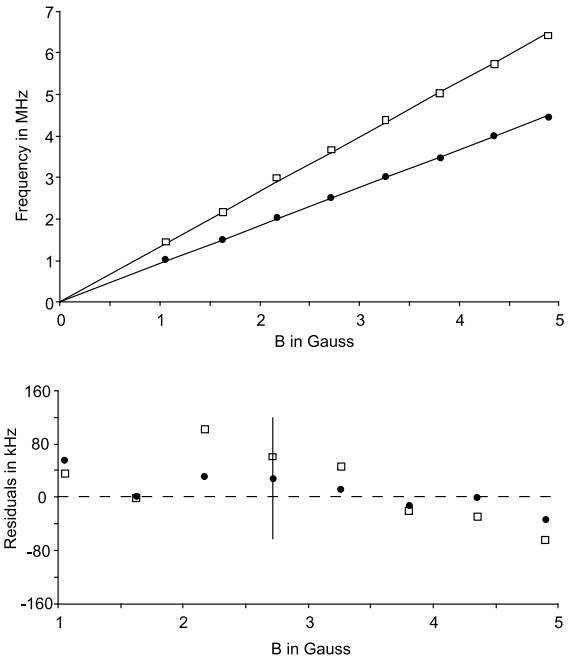

Fig. 3. Upper panel: Magnetic field dependence of the quantum beat frequencies for the $R_{21}(1)$ transition in the $v' = 1 \leftarrow v'' = 0$ band of OH. The lines mark linear fits to the data. Lower panel: Fit residuals.

$$\omega = 2\mu_B B g_F, \tag{2}$$

where $\mu_B = 1.39967$ MHz G^{-1}. An example for the $R_{21}(1)$ transition of the $v' = 1 \leftarrow v'' = 0$ band of OH is shown in Fig. 3, which includes the residuals to the linear fit and a typical error bar describing the uncertainty in our determination of the peak position.

For OD, hyperfine (zero-field) quantum beats were also observed, as initially reported by Huber and co-workers [53,54]. Fig. 4 displays a typical OD quantum beat spectrum, obtained for the $R_{21}(1)$ transition of the $v' = 1 \leftarrow v'' = 0$ band at a field strength of 2.72 G. A global least squares fit was performed to determine the Landé factors for each F component and the zero-field hyperfine splittings, from which the hyperfine coupling constants were determined as described below. The inter-manifold beat frequencies were fit using the formula:

$$\omega = \Delta + \mu_B B[M_F g_F - M_{F'} g_{F'}], \tag{3}$$

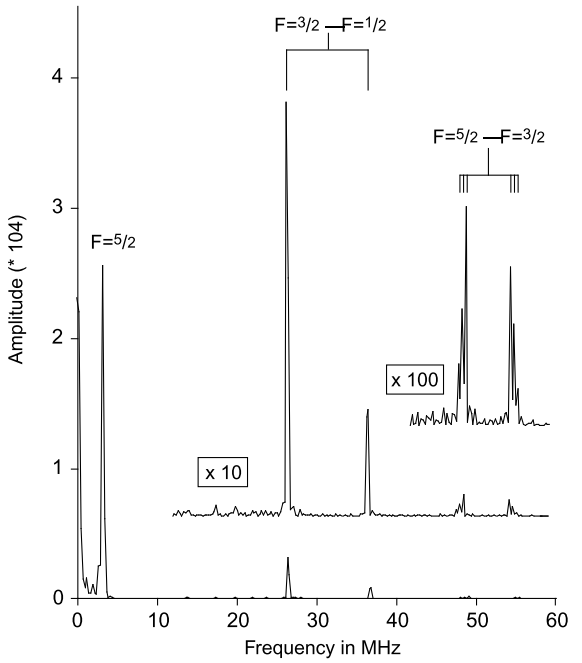

Fig. 4. Zeeman quantum beat spectrum of the $R_{21}(1)$ transition in the $v' = 1 \leftarrow v'' = 0$ band of OD at a field strength of 2.72 G. The intra- and inter-manifold beats are labeled in terms of the excited state hyperfine quantum numbers.

where Δ is the zero-field splitting of the two components F, F'. This procedure was followed for all transitions except $R_{11}(1)$, where the inter-manifold beats were particularly weak and difficult to observe above the noise. In this case, the zero-field splittings were obtained from a zero-field spectrum averaged over 5000 laser shots, and the Lande' factors were determined from the intra-manifold beats, following Eq. (2).

3. Theory and data modeling procedures

The $A^2\Sigma^+$ state of OH conforms to case $b_{\beta J}$ coupling [16,25,26], where $\mathbf{J} = \mathbf{N} + \mathbf{S}$ and $\mathbf{F} = \mathbf{J} + \mathbf{I}$, and $\mathbf{I} = \mathbf{I}_{H(D)}$. Consistent with previous treatments [22,25,26,33,38,40,42,53,54], for Zeeman experiments involving an unperturbed state with rotational angular momentum N the following Hamiltonian was assumed:

$$H = H_{sr} + H_{hfs} + H_Z, \tag{4}$$

where

$$H_{sr} = \gamma \mathbf{N} \cdot \mathbf{S} \tag{5}$$

is the spin–rotation interaction [25,26]. For OH the hyperfine Hamiltonian [88]:

$$H_{hfs} = b\mathbf{I} \cdot \mathbf{S} + cI_zS_z \tag{6}$$

was used, where b, c are the Frosch and Foley constants and the Fermi-contact interaction is given by $b + c/3$. For OD, the Hamiltonian included a quadripolar coupling term: [33,88]

$$H_{hfs} = b\mathbf{I} \cdot \mathbf{S} + cI_zS_z + eqQ\left[3I_z^2 - \frac{I(I+1)}{4I(2I-1)}\right]. \tag{7}$$

The effective Zeeman Hamiltonian for a diatomic molecule in a $^2\Sigma^+$ state can be expressed as: [89,90]

$$H_Z = g_s\mu_B B_0 T^1_{p=0}(\mathbf{S}) + g_l\mu_B B_0 \sum_{q=\pm1} D^{(1)}_{0q}(\omega) T^1_q(\mathbf{S}) - g_r\mu_B B_0 T^1_{p=0}(\mathbf{N}) - g_N\mu_N B_0 T^1_{p=0}(\mathbf{I}), \tag{8}$$

where the first term is the isotropic electron spin interaction, the second term represents anisotropic corrections to g_s, the third term accounts for the rotational Zeeman effect, and the final term represents the nuclear Zeeman effect. We included the nuclear Zeeman term in our analysis for both OH and OD.

The Hamiltonian matrix elements were evaluated in the case $b_{\beta J}$ basis. The hyperfine matrix elements were taken from Radford [88], using the correction noted by German [33], while the Zeeman matrix elements were taken from [90]. The Hamiltonian matrix was factored into submatrices for $J = N \pm 1/2$ and $F = J \pm 1/2$ (for $I = 1/2$) or $F = J + I, J + I - 1, \ldots, J - I$ (for $I = 1$). The matrix was of size 4×4 for OH, and for OD either 5×5 or 6×6. We used published spin–rotation constants for OD($v' = 0$–3) [30], and determined the hyperfine coupling constants b, c, and eQq by fitting the zero-field hyperfine splittings to values calculated by diagonalizing each submatrix with $B_0 = 0$. The diagonalization used a Jacobian transformation, and the fitting a least-squares routine. For OH, we used the hyperfine and spin–rotation constants for $v' = 0$ and 1 determined by ter Meulen et al. [44] and the parameters for $v' = 2$

were estimated from the energy dependence of the OD parameters. The rotational dependence of γ was neglected in our analysis, at it varies by only $\sim$0.2% over the range $N = 1$–3 [44].

We first diagonalized each submatrix at a single value of the field strength (B_0) in the range employed. Changing the value of B_0 in this range did not alter the calculated values, consistent with our observation of linear Zeeman tuning. The calculated Zeeman energies were averaged over all pairs of Zeeman sublevels of a given hyperfine component differing in M_F by 2, and divided by $\mu_B B_0$ to give the theoretical g_F factor. The calculated g_F factors were fit to the experimental values using a least-squares algorithm. In practice, we found that the data set did not allow simultaneous determination of the three g-factors: g_s, g_l, and g_r, a fact also noted by Carter et al. [54] in QBS studies of OD($\tilde{A}^2\Sigma^+, \upsilon = 0$). In that work, the value of g_r was constrained to be zero, since the predicted magnitude ($\sim$0.002) is around three times smaller than the value of g_l predicted from Curl's relationship. However, the matrix elements for this term are typically 4–5 times *larger* than those for g_l, and the relative contributions of these terms may thus be similar. We fixed g_s at the free electron value (2.002), and used g_l, and g_r as fit parameters, a procedure similar to that used by Raab et al. [42] in QBS studies of OH($\tilde{A}^2\Sigma^+, \upsilon' = 0$).

It is well known that fitted g-factors are sensitive to uncertainties in rotational constants and fine structure parameters [25,26,91]. For OD, the uncertainty in γ varies from $\sim$0.1% for $\upsilon' = 0$ to $\sim$9% for $\upsilon' = 3$ [30]. We conducted a series of fits of the data for OD($\upsilon' = 3$) to assess the sensitivity of the fitted values to uncertainties in γ and the hyperfine constants b, c, and eQq. Only the former produced a noticeable change, with the 9% uncertainty in γ leading to a 30% change in the fit value of g_l and 11% change in the fit value of g_r. These are significantly smaller than the experimental uncertainties.

4. Results and discussion

4.1. Zeeman parameters

Tables 1 and 2 list the experimental low field g_F-factors determined for various hyperfine levels in the $\upsilon' = 0$, 1, and 2 levels of OH($\tilde{A}^2\Sigma^+$) and the $\upsilon' = 0$, 1, 2, and 3 levels of OD($\tilde{A}^2\Sigma^+$). For OH($\upsilon' = 0$) (Table 1) the previous (and more precise) results of [42] are included for comparison. Due to the short lifetime of OH($\upsilon' = 2$), it was not possible to obtain data for the weak $S_{21}(1)$ transition, however, the data obtained for other rotational levels in this band is similar in precision to those for $\upsilon' = 0$ and 1, which demonstrates that QBS can be applied to the study of predissociating states.

Tables 3 and 4 list the fit values of g_l and g_r for OH($\upsilon' = 0$–2) and OD($\upsilon' = 0$–3), respectively. In a

Table 1
Experimental g_F-factors for the $A^2\Sigma^+$ state of OH

N	J	F	Experimental g_F factors			
			$\upsilon' = 0$[a]	$\upsilon' = 0$[b]	$\upsilon' = 1$[b]	$\upsilon' = 2$[b]
3	2.5	3	−0.2412(2)	−0.2397(9)	−0.2417(8)	[c]
		2	−0.3336(6)	−0.3338(26)	−0.3387(17)	[c]
2	2.5	3	0.3308(2)	0.3282(20)	0.3290(12)	0.3265(12)
		2	0.4701(6)	0.4747(30)	0.4754(22)	0.4743(33)
2	1.5	2	−0.3078(3)	−0.3087(17)	−0.3070(7)	−0.3103(34)
		1	−0.4991(6)	−0.5015(37)	−0.5011(24)	−0.5144(27)
1	1.5	2	0.4973(8)	0.4969(29)	0.5002(37)	0.4962(48)
		1	0.8649(14)	0.8633(49)	0.8807(90)	0.8819(75)

[a] Ref. [42].
[b] This work.
[c] Not determined.

Table 2
Experimental g_F-factors for the $A^2\Sigma^+$ state of OD

N	J	F	Experimental g_F factors			
			$v' = 0$	$v' = 1$	$v' = 2$	$v' = 3$
3	2.5	3.5	−0.2022(16)	−0.2020(10)	−0.2036(18)	−0.2052(28)
		2.5	−0.2582(23)	−0.2631(25)	−0.2594(20)	−0.2662(34)
		1.5	−0.4061(28)	−0.4020(30)	−0.4097(35)	−0.4176(55)
2	2.5	3.5	0.2786(11)	0.2799(15)	0.2841(21)	0.2815(18)
		2.5	0.3603(20)	0.3600(34)	0.3663(29)	0.3658(39)
		1.5	0.5659(40)	0.5681(35)	0.5735(43)	0.5696(41)
2	1.5	2.5	−0.2434(14)	−0.2407(10)	−0.2459(12)	−0.2459(17)
		1.5	−0.2994(29)	−0.2996(49)	−0.2936(96)	−0.303(11)
		0.5	−0.666(18)	−0.665(16)	−0.685(30)	−0.675(34)
1	1.5	2.5	0.3982(17)	0.3988(19)	0.4059(30)	0.4015(24)
		1.5	0.5020(94)	0.5064(64)	0.510(17)	0.510(11)
		0.5	1.141(30)	1.141(24)	1.140(55)	1.139(36)

Table 3
Zeeman parameters for the $A^2\Sigma^+$ state of OH

v'	g_s[a]	g_l	g_r	σ[b]
0	2.002	−0.020(10)	0.0035(22)	0.0035
1	2.002	−0.002(8)	0.0013(18)	0.0028
2	2.002	0.007(13)	0.0056(33)	0.0041

[a] Fixed.
[b] Standard deviation of the fit.

Table 4
Zeeman parameters for the $A^2\Sigma^+$ state of OD

v'	g_s[a]	g_l	g_r	σ[b]
0	2.002	−0.001(8)	0.001(2)	0.0041
1	2.002	0.000(8)	0.000(2)	0.0040
2	2.002	0.016(11)	0.002(2)	0.0053
3	2.002	0.010(10)	0.004(2)	0.0049

[a] Fixed.
[b] Standard deviation of the fit.

two-state model, g_l can be predicted from the perturbation treatment of Curl [81]

$$g_l \cong -\frac{\gamma}{2\tilde{B}}. \quad (9)$$

Using the reported constants [9,27,44], the calculated value for ($\tilde{A}^2\Sigma^+$, $v' = 0$) is $\sim$−0.007. Our experimental results for OH $\{g_l = -0.020(10)\}$ and OD$\{g_l = -0.001(8)\}$ bracket this value. To increase the precision, we conducted a global fit of the OH and OD values, using the appropriate dependence on reduced mass for g_r. The value derived from this fit, $g_l = -0.007(7)$ (Table 5), is in good agreement with that calculated from Eq. (9).

Our fit value of g_l for OD($v' = 0$) is much smaller than that of Carter et al. [54] who report $g_l = -0.095(41)$. This discrepancy does not arise from the analysis procedure, as when fitting our results with g_r set to 0.0 we derive g_l and g_s values of 0.004(36) and 1.997(35), respectively. Although Carter et al. [54] did not include the nuclear Zeeman effect in their analysis, we find that the magnitude of this effect for OD is at the precision of our measurements, and thus cannot account for the discrepancy. We have also not identified any systematic error (field calibration, etc.) that could reasonably explain this result, and thus at present the origin of this discrepancy remains unexplained.

If g_l was determined solely via coupling with $\tilde{X}^2\Pi$, its value should not depend on v', since the second-order contribution that gives rise to γ is proportional to $\tilde{B}$. Indeed, the observed decrease in γ with increasing v' in OD($\tilde{A}^2\Sigma^+$), from 0.12010(12) cm^{-1} for $v' = 0$ to 0.106(9) cm^{-1} for $v' = 3$, closely

Table 5
Zeeman parameter values for the combined fits

v' (OH/OD)	g_s[a]	g_l	g_r	σ[b]
0/0	2.002	−0.007(7)	0.0028(25)	0.0045
2/3	2.002	0.011(9)	0.0056(38)	0.0055

[a] Fixed.
[b] Standard deviation of the fit.

mirrors the decrease in $\tilde{B}$, from 9.04351(12) cm^{-1} for $v' = 0$ to 8.0746(5) for $v' = 3$ [30]. Our results, in contrast, show that with increasing v', g_l changes sign (Tables 3 and 4), although the effect is near the limit of our experimental precision. The upper panel of Fig. 5 displays a combined plot of the vibrational energy dependence of g_l for OH and OD in the $\tilde{A}^2\Sigma^+$ state. To better resolve this trend, as noted above we conducted a simultaneous fit of the g-factors for OH and OD levels lying close in energy $\{v' = 0$ (OH) with $v' = 0$ (OD), and $v' = 2$ (OH) with $v' = 3$ (OD)$\}$, and the derived parameters are listed in Table 5.

Turning to the rotational g-factor (g_r), the values determined for OH($v' = 0$) and from a simultaneous fit of the $v' = 0$ data for OH and OD are consistent with the (more precise) value of 0.00248(6) determined by Raab et al. [42] and with calculations based on coupling to $\tilde{X}^2\Pi$ [42]. The lower panel of Fig. 5 shows the vibrational energy dependence of g_r for OH and OD in the $\tilde{A}^2\Sigma^+$ state. It appears that g_r increases at higher energies (Tables 3–5), but the trend is not outside our experimental uncertainty.

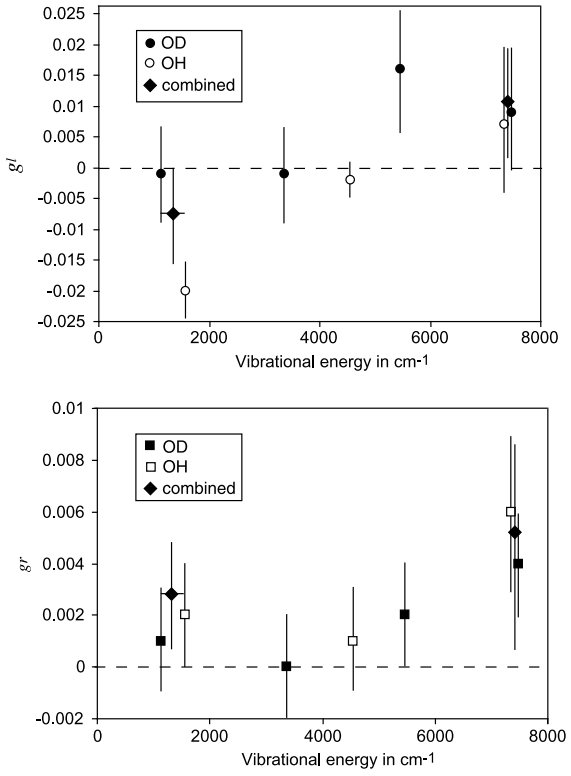

Fig. 5. Upper panel: Fit values of g_l for OH, OD, and the combined fits plotted against vibrational energy in the $\tilde{A}^2\Sigma^+$ state. Lower panel: Similar plot for g_r.

We considered several explanations for the observed energy dependence of g_l, which are summarized below.

4.1.1. Interactions with higher lying Π states

A change in sign of g_l could arise from interactions with higher lying Π states, leading to a change in sign of the energy denominator in the second-order contribution: [89–92]

$$g_l^e \cong \sum_{\Pi} \frac{\langle \Pi | AL^+ | \Sigma \rangle \langle \Sigma | L^+ | \Pi \rangle}{E_\Sigma - E_\Pi}. \tag{10}$$

Candidates include $2^2\Pi$, which correlates to $O(^1D) + H(^2S)$ and is calculated to lie ~48,000 cm^{-1} above $\tilde{A}^2\Sigma^+$ [61], and the repulsive $1^4\Pi$ state, which correlates to $O(^3P) + H(^2S)$ and lies slightly higher than $2^2\Pi$ in the Franck–Condon region [61,67]. The $1^4\Pi$ state should be more important, as the configuration of this state differs from that of $\tilde{A}^2\Sigma^+$ by one spin–orbital [93]. Using the ab initio potential curves and spin–orbit matrix element at $R = 2.0$ bohr [67,73], from which a value for $\langle \Pi | AL^+ | \Sigma \rangle$ of ~200 cm^{-1} is derived [93], we estimate a contribution to g_l from the $\tilde{A}^2\Sigma^+$–$1^4\Pi$ interaction of ~0.007 for the highest v'.

4.1.2. Interactions with higher lying Σ state(s)

Interactions with the higher lying $1^4\Sigma^-$ state can influence g_l via the third-order term: [92]

$$g_l^{e(3)} \cong -\sum_{^4\Sigma} \frac{\langle ^2\Sigma | H_{SO} | ^4\Sigma \rangle^2}{\left[E_{^2\Sigma} - E_{^4\Sigma}\right]^2}. \tag{11}$$

However, as the sign of this term is negative, it would lead to a *decrease* in g_l. Moreover, given the calculated spin–orbit matrix element (H_{SO}) between $\tilde{A}^2\Sigma^+$ and $1^4\Sigma^-$ in the Franck–Condon region (−2.2 cm^{-1} at $R = 2.00$ bohr) [67,73], the contribution from this term is negligibly small.

4.1.3. Modification of g_s via interactions with higher lying states

In our analysis, we fixed g_s at the free electron value. This might not be a good assumption, as

interactions with $2^2\Pi$ and $1^4\Pi$ can modify g_s via the third order term [92,94]:

$$g_s^{(3)} \cong -\sum_{\Pi} \frac{|\langle \Pi | H_{SO} | \Sigma \rangle|^2}{[E_\Sigma - E_\Pi]^2}. \quad (12)$$

However, as the sign of this term is negative, neglecting it should produce a *decrease* in the fit value of g_l. Moreover, based upon the ab initio matrix elements [67,73], these terms are negligibly small in the Franck–Condon region.

On the basis of these considerations, we suggest that the energy dependence of g_l may reflect the $\tilde{A}^2\Sigma^+ - 1^4\Pi$ interaction, which is known to lead to predissociation at higher energies. The estimated contribution to g_l is of the correct sign and order of magnitude; however, it is curious that this effect should not be manifest in the $\tilde{A}^2\Sigma^+$ spin–rotation constants [30], and at present we have no explanation for this. Further analysis would benefit from additional calculations, particularly of the radial dependence of the L^+ matrix element, and additional experiments encompassing a larger range of N, which would allow a more precise determination of the energy dependence of g_r [42].

4.2. Hyperfine parameters

Table 6 lists the experimental hyperfine splittings determined in this work for OD($\tilde{A}^2\Sigma^+, v' =$ 0–3), and compared with the results of Carter et al. [54] for $v' = 0$. Table 7 compares the determined hyperfine parameters (b, c, eQq and the Fermi-contact constant $b + c/3$) with previous measurements and theoretical predictions for $v' = 0$ and 1. Our results are generally in good agreement with the QBS measurements of Carter et al. [54] and previous experimental studies [25,26,33].

The Fermi-contact hyperfine constant ($b + c/3$) is proportional to the spin density of the unpaired electron, $|\psi(0)|^2$, at the deuterium nucleus. As the O–D bond is stretched, this term should approach the value for the $^2\mathbf{S}$ state of atomic deuterium, which is 218.256 MHz [95]. Thus, an increase in

Table 7
Hyperfine parameters (in MHz) for the $A^2\Sigma^+$ state of OD

v'	b	c	$b + c/3$	eqQ
0[a]	110.182(20)	24.72(11)	118.42	0.238(30)
0[b]	109.73(5)	25.73(20)	118.31(14)	0.22(5)
0[c]	110.18(3)	24.85(17)	118.46(7)	0.29(5)
0[d]	112.7	25.4	121.2	0.262
1[b]	111.15(5)	24.40(20)	119.28(14)	0.05(4)
1[c]	111.29(5)	23.81(24)	119.23(10)	0.20(10)
1[d]	115.7	24.3	123.8	0.258
2[c]	112.63(8)	22.78(40)	120.22(14)	0.30(13)
3[c]	114.49(8)	21.40(39)	121.62(15)	0.31(13)

[a] Experiment [54].
[b] Experiment [33].
[c] Experiment, this work.
[d] Theory [59].

Table 6
Experimental hyperfine level splittings (in MHz) for the $A^2\Sigma^+$ state of OD

N	J	F'	F''	Experimental hyperfine level splittings in MHz				
				$v' = 0$[a]	$v' = 0$[b]	$v' = 1$	$v' = 2$	$v' = 3$
3	2.5	3.5	2.5	52.90	52.84(3)	53.50(4)	54.37(4)	55.44(4)
		2.5	1.5	37.86	37.91(2)	38.49(3)	38.94(3)	39.72(4)
2	2.5	3.5	2.5	78.55	78.58(2)	79.25(3)	80.02(4)	81.13(4)
		2.5	1.5	57.18	57.31(3)	57.72(2)	58.34(4)	59.17(4)
2	1.5	2.5	1.5	51.40	51.35(2)	52.02(2)	52.85(2)	54.04(3)
		1.5	0.5	31.03	31.10(3)	31.57(2)	32.10(2)	32.76(2)
1	1.5	2.5	1.5	94.37	94.29(3)	95.04(3)	96.00(4)	97.32(4)
		1.5	0.5	58.50	58.71(2)	59.16(3)	59.76(4)	60.56(3)

Not determined.
[a] Ref. [54].
[b] This work.

this term with increasing v' is expected, and clearly observed (Table 7). The calculations [59] reproduce this trend but overestimate its magnitude, predicting a ~2% increase in going from $v' = 0$–1, while the experiment shows an increase of only ~0.7%. Ter Meulen et al. [44] observed a similar trend for OH, with $b + c/3$ increasing by ~0.2% in going from $v' = 0$–1.

The parameter c represents the dipole–dipole interaction, given by: [88]

$$c = 3g_e g_I \mu_B \mu_N \left\langle \frac{P_2(\cos\theta)}{r^3} \right\rangle, \tag{13}$$

where g_e and g_I are the electron and nuclear g-factors, μ_B and μ_N are the Bohr and nuclear magneton, the argument of the Legendre polynomial $P_2(x) = (3x^2 - 1)/2$ is the cosine of the angle of the electron coordinate with respect to the internuclear axis, and r is the distance between the electron and the nucleus of spin I. For OH, ter Meulen et al. [44] observed a significant (~10%) decrease in c in going from $v' = 0$–1. We find a decrease of ~4% for OD, in reasonable agreement with the results of German [33] and theoretical predictions [59]. This trend continues to higher energy, with a total decrease of ~14% in going from $v' = 0$–3.

The magnitude of c is usually interpreted in terms of a p orbital on the nucleus in question; however, for protons the p orbital lies too high in energy to contribute, and the dominant contribution comes from interaction of the deuterium nucleus with the oxygen atom unpaired spin-density [96]. Indeed, the ground state c constants in a series of XH radicals approximately scale with the inverse cube of the equilibrium internuclear separation (r_e) [96]. As a simple test of this hypothesis, we plot in Fig. 6 the experimental values for c versus the inverse cube of the average value of the internuclear separation r approximated from the data of Coxon [30]. The graph is linear to within our experimental precision, and a fit using linear regression is shown as the solid line in Fig. 6.

In contrast to b and c, the small quadrupolar coupling constant eQq is not well determined, and no obvious dependence on energy is found to within our experimental precision. Our findings are consistent with theoretical predictions [59], and

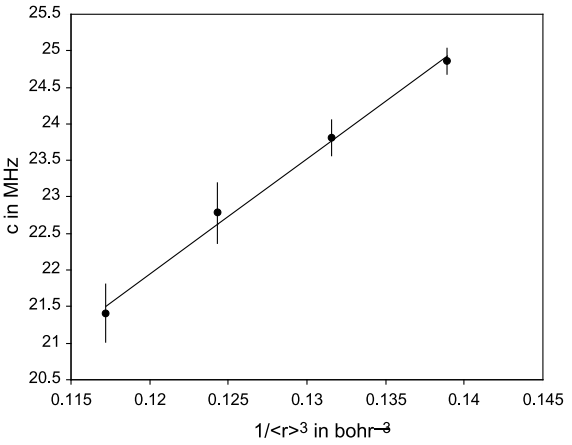

Fig. 6. Fit values for the dipole–dipole hyperfine constant c of OD($\tilde{A}^2\Sigma^+, v' = 0$–3) plotted against the inverse cube of the average internuclear separation approximated from the data of [30]. The solid line marks a linear fit.

do not support the sharp (~4 fold) drop in eQq from $v' = 0$–1 reported by German [33]. For further analysis, it is highly desirable to have ab initio predictions of the trend in hyperfine parameters for $v' > 1$.

5. Conclusions

We have examined the energy dependence of the Zeeman parameters in the $\tilde{A}^2\Sigma^+$ state of OH and OD, and the nuclear hyperfine parameters for OD, using the technique of quantum beat spectroscopy. We find that the sign and magnitude of the anisotropic g-factor g_l for $v' = 0$ is consistent with that expected from Curl's relationship, but at higher energies this factor appears to change sign. The rotational g-factor g_r is not well determined and its energy dependence is not well characterized; however, its magnitude is consistent with previous results and theoretical expectations. We examined several explanations for the observed energy dependence of g_l, and conclude that the most likely involves interaction of $\tilde{A}^2\Sigma^+$ with the higher lying $^4\Pi$ state, which is known to lead to predissociation at higher energies. We also determined the magnetic and electric quadrupole hyperfine constants for OD($\tilde{A}^2\Sigma^+$, $v' = 0$–3), the constants for $v' = 2$, 3 being reported here for the

first time, and the derived values are consistent with previous experimental results and available ab initio calculations.

Acknowledgements

The authors gratefully acknowledge useful discussions with J.M. Brown and R.N. Zare. This work was supported by the National Science Foundation under Grant CHE-9702803.

References

[1] G. Herzberg, Molecular Spectra and Molecular Structure I. Spectra of Diatomic Molecules, Van Nostrand, Princeton, 1950.
[2] G. Herzberg, The Spectra and Structures of Simple Free Radicals, Cornell University Press, Ithaca, 1971.
[3] A.G. Gaydon, H.G. Wolfhard, Proc. R. Soc. A 208 (1951) 63.
[4] H.P. Broida, W.R. Kane, Phys. Rev. 89 (1953) 1053.
[5] G.C. Dousmanis, T.M. Sanders Jr., C.H. Townes, Phys. Rev. 100 (1955) 1735.
[6] G. Ehrenstein, C.H. Townes, M.J. Stevenson, Phys. Rev. Lett. 3 (1959) 40.
[7] H.E. Radford, Phys. Rev. 122 (1961) 114.
[8] H.E. Radford, Phys. Rev. 126 (1962) 1035.
[9] G.H. Dieke, H.M. Crosswhite, J. Quant. Spectrosc. Radiat. Transfer 2 (1963) 97.
[10] H.E. Radford, Phys. Rev. Lett. 13 (1964) 534.
[11] R.L. Poynter, R.A. Beaudet, Phys. Rev. Lett. 21 (1968) 305.
[12] H.B. Palmer, D.W. Naegeli, J. Mol. Spectrosc. 28 (1968) 417.
[13] P. Felenbok, Ann. Astrophys. 26 (1963) 393.
[14] C. Carlone, F.W. Dalby, Can. J. Phys. 47 (1969) 1945.
[15] A. Marshall, R.L. deZafra, H. Metcalf, Phys. Rev. Lett. 22 (1969) 445.
[16] K.R. German, R.N. Zare, Bull. Am. Phys. Soc. 15 (1970) 82.
[17] K.M. Evenson, J.S. Wells, H.R. Radford, Phys. Rev. Lett. 25 (1970) 199.
[18] A. Carrington, N.J.D. Lucas, Proc. R. Soc. A 314 (1969) 567.
[19] A. Churg, D.H. Levy, Astrophys. J. 162 (1970) L161.
[20] P.M. Clough, A.H. Curran, B.A. Thrush, Proc. R. Soc. A 323 (1971) 541.
[21] K.P. Lee, W.G. Tam, R. Larouche, G.A. Woonton, Can. J. Phys. 49 (1971) 2207.
[22] R.L. deZafra, A. Marshall, H. Metcalf, Phys. Rev. A 3 (1971) 1557.
[23] E.A. Scarl, F.W. Dalby, Can. J. Phys. 49 (1971) 2825.
[24] B.G. Elmergreen, W.H. Smith, Astrophys. J. 178 (1972) 557.
[25] K.R. German, T.H. Bergeman, E.M. Weinstock, R.N. Zare, J. Chem. Phys. 58 (1973) 4304.
[26] E.M. Weinstock, R.N. Zare, J. Chem. Phys. 58 (1973) 4319.
[27] M.A.A. Clyne, J.A. Coxon, A.R. Woon Fat, J. Mol. Spectrosc. 46 (1973) 146.
[28] J.H. Brophy, J.A. Silver, J.L. Kinsey, Chem. Phys. Lett. 28 (1974) 418.
[29] K.R. German, J. Chem. Phys. 63 (1975) 5252.
[30] J.A. Coxon, J. Mol. Spectrosc. 58 (1975) 1.
[31] J.A. Coxon, R.E. Hammersley, J. Mol. Spectrosc. 58 (1975) 29.
[32] D. Wilcox, R. Anderson, J. Peacher, J. Opt. Soc. Am. 65 (1975) 1368.
[33] K.R. German, J. Chem. Phys. 64 (1976) 4192.
[34] D.K. Killinger, C.C. Wang, M. Hanabusa, Phys. Rev. A 13 (1976) 2145.
[35] J.L. Destombes, C. Marliere, F. Rohart, J. Mol. Spectrosc. 67 (1977) 93.
[36] J.M. Brown, M. Kaise, C.M.L. Kerr, D.J. Milton, Mol. Phys. 36 (1978) 553.
[37] J. Brzozowski, P. Erman, M. Lyyra, Phys. Scr. 17 (1978) 507.
[38] P. Lebow, F. Raab, H. Metcalf, Phys. Rev. Lett. 42 (1979) 85.
[39] J.J. ter Meulen, G.W.M. van Mierlo, A. Dymanus, Phys. Rev. Lett. 43 (1979) 29.
[40] F. Raab, T. Bergeman, D. Lieberman, H. Metcalf, Opt. Lett. 5 (1980) 427.
[41] T. Bergeman, P. Erman, Z. Haratym, M. Larsson, Phys. Scr. 23 (1981) 45.
[42] F. Raab, T. Bergeman, D. Lieberman, H. Metcalf, Phys. Rev. A 24 (1981) 3120.
[43] J.A. Coxon, S.C. Foster, J. Mol. Spectrosc. 91 (1982) 243.
[44] J.J. ter Meulen, W.A. Majewski, W.L. Meerts, A. Dymanus, Chem. Phys. Lett. 94 (1983) 25.
[45] K.I. Peterson, G.T. Fraser, W. Klemperer, Can. J. Phys. 62 (1984) 1502.
[46] P. Andresen, A. Bath, W. Groger, H.W. Luelf, G. Meijer, J.J. ter Meulen, Appl. Opt. 27 (1988) 365.
[47] D.D. Nelson Jr., A. Schiffman, D.J. Nesbitt, D.J. Yaron, J. Chem. Phys. 90 (1989) 5443.
[48] A. Arnold, W. Ketterle, J. Wolfrum, Appl. Phys. B 51 (1990) 99.
[49] T. Dreier, D.J. Rakestraw, Appl. Phys. B 50 (1990) 475.
[50] J.A. Gray, R.L. Farrow, J. Chem. Phys. 95 (1991) 7054.
[51] K.P. Huber, F. Holland, J.A. Coxon, J. Chem. Phys. 96 (1992) 1005.
[52] D.E. Heard, D.R. Crosley, J.B. Jeffries, G.P. Smith, A. Hirano, J. Chem. Phys. 96 (1992) 4366.
[53] I.M. Povey, R.T. Carter, H. Bitto, J.R. Huber, Chem. Phys. Lett. 248 (1996) 470.
[54] R.T. Carter, I.M. Povey, H. Bitto, J.R. Huber, J. Chem. Phys. 104 (1996) 5365.
[55] J.J.L. Spaanjaars, J.J. ter Meulen, G. Meijer, J. Chem. Phys. 107 (1997) 2242.

[56] A.A. Suvernev, R. Tadday, T. Drier, Phys. Rev. A 58 (1998) 4102.
[57] J. Czarny, P. Felenbok, H. Lefebvre-Brion, J. Phys. B 4 (1971) 124.
[58] A.G. Gaydon, I. Kopp, J. Phys. B 4 (1971) 752.
[59] S. Green, J. Chem. Phys. 58 (1973) 4327.
[60] M.L. Sink, A.D. Bandrauk, Chem. Phys. Lett. 65 (1979) 246.
[61] E.F. van Dishoeck, A. Dalgarno, J. Chem. Phys. 79 (1983) 873.
[62] S.R. Langhoff, H. Partridge, J. Mol. Spectrosc. 105 (1984) 261.
[63] E.F. van Dishoeck, M.C. van Hemert, A.C. Allison, A. Dalgarno, J. Chem. Phys. 81 (1984) 5709.
[64] S.J. Singer, K.F. Freed, Y.B. Band, Adv. Chem. Phys. 61 (1985) 1.
[65] S. Lee, C.J. Williams, K.F. Freed, Chem. Phys. Lett. 130 (1986) 271.
[66] S. Lee, K.F. Freed, J. Chem. Phys. 87 (1987) 5772.
[67] D.R. Yarkony, J. Chem. Phys. 97 (1992) 1838.
[68] S. Lee, Chem. Phys. Lett. 240 (1995) 595.
[69] S. Lee, Chem. Phys. Lett. 243 (1995) 250.
[70] S. Lee, J. Phys. Chem. 99 (1995) 13380.
[71] S. Lee, J. Chem. Phys. 103 (1995) 3501.
[72] S. Lee, J. Chem. Phys. 104 (1996) 1912.
[73] G. Parlant, D.R. Yarkony, J. Chem. Phys. 110 (1999) 363.
[74] M.P. de Lara Castells, A. Mitrushenkov, P. Palmieri, F. le Quèrè, C. Leonard, P. Rosmus, Mol. Phys. 98 (2000) 1713.
[75] M. Glass-Maujean, J. Breton, P.M. Guyon, Chem. Phys. Lett. 63 (1979) 591.
[76] J.T. Brandon, S.A. Reid, D.C. Robie, H. Reisler, J. Chem. Phys. 97 (1992) 5246.
[77] S.A. Reid, J.T. Brandon, H. Reisler, J. Phys. Chem. 97 (1993) 540.
[78] B. Kim, K. Yoshihara, J. Chem. Phys. 99 (1993) 1433.
[79] B. Kim, K. Yoshihara, S. Lee, Phys. Rev. Lett. 73 (1994) 424.
[80] B.R. Lewis, S.S. Banerjee, S.T. Gibson, J. Chem. Phys. 102 (1995) 6631.
[81] R.F. Curl, Mol. Phys. 5 (1965) 585.
[82] Y. Tang, J.P. Schmidt, S.A. Reid, J. Chem. Phys. 110 (1999) 5734.
[83] Ju Xin, S.A. Reid, J. Chem. Phys. 112 (2000) 10067.
[84] J. Xin, S.A. Reid, F. Santoro, C. Petrongolo, J. Chem. Phys. 115 (2001) 8868.
[85] J. Xin, S.A. Reid, J. Chem. Phys. 116 (2002) 515.
[86] R.T. Carter, J.R. Huber, Chem. Soc. Rev. 29 (2000) 305.
[87] J. Xin, H. Fan, I. Ionescu, D. Kuffel, S.A. Reid, J. Mol. Spectrosc. 219 (2003) 37.
[88] H.E. Radford, Phys. Rev. A 136 (1964) 1571.
[89] A. Carrington, D.H. Levy, T.A. Miller, Adv. Chem. Phys. 18 (1970) 149.
[90] I.C. Bowater, J.M. Brown, A. Carrington, Proc. R. Soc. London, Ser. A 333 (1973) 265.
[91] L. Veseth, J. Mol. Spectrosc. 63 (1976) 180.
[92] H. Christensen, L. Veseth, J. Mol. Spectrosc. 72 (1978) 438.
[93] H. Lefebvre-Brion, R.W. Field, Perturbations in the spectra of diatomic molecules, Academic Press, Orlando, 1986.
[94] J.M. Brown, K. Dumper, C.R. Parent, Mol. Phys. 36 (1978) 1149.
[95] J.E. Nafe, E.B. Nelson, Phys. Rev. 73 (1948) 718.
[96] E. Hirota, High-resolution Spectroscopy of Transient Molecules, Springer, Berlin, 1985.